# Non-inertial lateral migration of vesicles in bounded Poiseuille flow

Gwennou Coupier,[1, *] Badr Kaoui,[1, 2] Thomas Podgorski,[1] and Chaouqi Misbah[1]

[1]*Laboratoire de Spectrométrie Physique, CNRS - UMR 5588,*
*Université Grenoble I, B.P. 87, 38402 St Martin d'Hères Cedex, France*
[2]*Université Hassan II - Mohammedia, Faculté des Sciences Ben M'Sik,*
*Laboratoire de Physique de la Matière Condensée, BP 7955 Casablanca, Morocco*
(Dated: October 28, 2008)

Cross-streamline non-inertial migration of a vesicle in a bounded Poiseuille flow is investigated experimentally and numerically. The combined effects of the walls and of the curvature of the velocity profile induce a movement towards the center of the channel. A migration law (as a function of relevant structural and flow parameters) is proposed that is consistent with experimental and numerical results. This similarity law markedly differs from its analogue in unbounded geometry. The dependency on the reduced volume $\nu$ and viscosity ratio $\lambda$ is also discussed. In particular, the migration velocity becomes non monotonous as a function of $\nu$ beyond a certain $\lambda$.

Flow of confined soft entities, such as vesicles (closed quasi-inextensible lipid membranes), or blood cells in the circulatory system and in microfluidic devices, is a problem of a paramount importance with both fundamental and practical interests. While inertial effects can induce lateral migration of any flowing body in a channel [1, 2, 3], the ability of these soft entities to adapt their shapes under non-equilibrium conditions gives them the possibility to migrate transversally even at low Reynolds number. Transverse migrations induce non uniform lateral distributions of the suspended entities, which has important consequences on the rheology of a confined suspension (e.g. the Fahraeus-Lindquist effect in blood vessels [4]), or should impact on transport efficiency in the various sorting microfluidic devices that are now being developed [5].

Despite the considerable interest for transverse migration in many circumstances, there is, to our knowledge, yet no quantitative law that would allow one to relate the lateral migration velocity of a deformable entity flowing in a channel, even isolated, with its position, its mechanical properties, and the flow parameters. We propose a law for the case of a single vesicle placed in a bounded Poiseuille flow, from experiments in microfluidic devices as well as simulations based on the boundary integral method.

The behavior of vesicles under unbounded shear flow has been the subject of several theoretical [6, 7, 8, 9, 10] and experimental [11, 12, 13] studies. When the viscosity ratio between the inner and the outer fluids is small, vesicles perform a tank treading dynamics where the orientation of the main axis of the vesicle is constant and the membrane undergoes a tank treading motion. In a bounded Poiseuille flow, tank-treading vesicles experience a transverse force and reach the center where they assume a steady shape. The latter stage has been described in several papers [14, 15, 16]. Migration in Poiseuille flows has been also reported on capsules [17, 18, 19], red blood cells [18, 19], and drops [20, 21]. The latter seem to have a very different behavior: depending on the viscosity ratio and the confinement, the reported equilibrium positions are not always on the centerline. In addition, a drop interface and a vesicle membrane are mechanically different: a vesicle has a constant surface area and its equilibrium shape is not a sphere in general. As a consequence of these intrinsic differences the vesicle shape under flow is described (in the co-moving frame), to leading order, by a nonlinear shape equation while a drop obeys a linear equation [8].

Lateral migration has two distinct sources. (i) A wall-induced lift force [22, 23, 24, 25]. In agreement with the numerical and theoretical studies for simple shear flows [22, 24], we showed recently that the migration velocity decreases like $1/y^2$, where $y$ is the distance to the wall of the center of mass of the vesicle [26]. (ii) The non-constant shear rate in a parabolic velocity profile (even unbounded) leads to a subtle interplay between the gradient of shear and the shape [27], resulting in migration towards the center with a constant drift velocity except near the center-line. In a realistic channel, both effects coexist and we shall see that this leads to a new and nontrivial non-inertial migration law.

The considered microfluidic channel is straight and has a rectangular cross section. The flow direction is $Ox$, and we investigate lateral migration along $Oy$. Let $2w$ denote the channel width in the $y$-direction, and $v_0$ the imposed flow velocity at the center of the channel in the absence of vesicle. The two walls are located at $y = 0$ and $y = 2w$.

A vesicle is characterized by two geometrical parameters: its effective radius $R_0$, determined from its constant volume $\mathcal{V}$ by $R_0 = (3\mathcal{V}/4\pi)^{1/3}$, and its reduced volume $\nu = \mathcal{V}/[4\pi(\mathcal{S}/4\pi)^{3/2}/3]$ ($\mathcal{S}$ is the constant area of the vesicle) characterizing vesicle deflation. Volumes are calculated at lift-off (see below) by assuming axisymmetric shape about the vesicle's main axis. The viscosity ratio is defined as $\lambda = \eta_{in}/\eta_{out}$, where $\eta_{in}, \eta_{out}$ denote the inner and the outer viscosities. Relevant space and time scales are the vesicle radius $R_0$ and the characteristic time needed by the vesicle to relax to its equilibrium
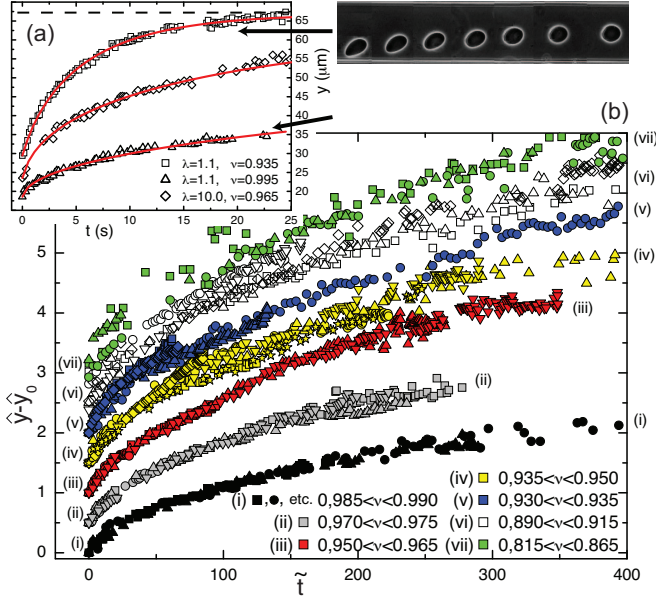
FIG. 1: (color online) (a): Experimental time evolution of the lateral position $y$ for 3 vesicles of similar size ($19\pm1\,\mu$m) and imposed flow velocity $v_0 = 920\,\mu$m.s$^{-1}$ but different $\nu$ and $\lambda$. The dashed line indicates the center-line (which will be reached much later by two of the vesicles). The solid line shows the $y(t)$ curve obtained from the fit by the numerical solution of Eq. 1. (b): Evolution of $\hat{y} - \hat{y}_0$ versus $\tilde{t}$ for vesicles with $\lambda = 1.1$ and different $\nu$. For each $\nu$ interval, the different symbols correspond to different vesicles, whose $\hat{w}$ and $\hat{v}_0$ vary in the explored intervals, that are $1.8 < \hat{w} < 9.6$ and $400 < \hat{v}_0 < 14800$. The corresponding curves clearly collapse on a single one. For clarity, the sets of curves corresponding to different $\nu$ intervals are switched vertically with an increment of 0.5.

shape (in the absence of imposed flow), which is given by $\tau = \eta_{out} R_0^3/\kappa$, where $\kappa \sim 20 k_B T$ is the membrane's bending rigidity (typically, $\tau \sim 10$ s).

Therefore dynamics depends a priori on the four dimensionless parameters ($\hat{w} \equiv w/R_0$, $\hat{v}_0 \equiv v_0\tau/R_0$, $\nu$, $\lambda$). We consider first the case $\lambda \simeq 1$. The strategy is to vary $\hat{w}$ and the imposed velocity $\hat{v}_0$ and investigate the migration law $\hat{y}(\hat{t}) = y(t/\tau)/R_0$ for each value of $\nu$. Then we discuss the influence of $\nu$ and $\lambda$.

In the experiments, we used straight channels of height $h_0 = 66.6\,\mu$m (in the direction of gravity $z$) and width $2w$ (rectangular cross section) between 70 and 140 $\mu$m. The walls of the channels are made of PDMS glued to a glass slide. The flow is induced by gravity, by connecting the inlet and the outlet to reservoirs at different heights. Vesicles are prepared following the electroformation method. They are made of a dioleoylphosphatidylcholine (DOPC) lipid bilayer enclosing an inner solution of sugar (sucrose or glucose) in water or in a 1:4 glycerol-water (w:w) mixture. Samples are diluted in a slightly hyperosmotic outer solution of the same type, in order to deflate them by osmosis. Dextran can be added to one of the solutions to modify the viscosity ratio $\lambda$. Vesicle size

$R_0$ lies in the range 7-37 $\mu$m while $v_0$ varies between 200 and 1100 $\mu$m.s$^{-1}$. Note that for our solutions of viscosity and density close to the one of water, the Reynolds number $R_e = \rho v_0 R_0/\eta_{out}$ is always lower than $4.10^{-2}$.

A particular design of the upstream channel creates an initial condition where incoming vesicles touch the $y = 0$ wall in the observation area and start to be lifted away from it. In particular, they have already developed a nearly ellipsoidal shape tilted with respect to the wall [23, 24, 25]. The 2D fluid velocity profile in the $xy$ plane where their center of mass lies is nearly parabolic, since the rectangular cross section of the 3D channel obeys $2w/h_0 \leq 3$ [28]. Moreover, we wait for the flow to be established for a long time, resulting in preliminary centering of the vesicles in the $z$ direction. The imposed velocity profile is thus written as $v_x^\infty(\mathbf{r}) = c\left(yw - y^2/2\right)$, where $c = 2v_0/w^2$ is the curvature. A vesicle is tracked along its trajectory with a phase contrast microscope, and the position $y$ of its center of mass is determined by image processing, starting with $y(t = 0) = y_0$, where $y_0$ is the position just before lift-off, which is close to $R_0$.

The evolution with time of the $y$ position of two vesicles with $\lambda = 1.1$ is shown in Fig. 1(a). The vesicles quickly move away from the wall, then the migration velocity decreases to zero as they approach the center-line. Along their trajectory, they continuously deform from a tilted ellipsoid to a symmetric bullet-like shape. For a given $\nu$, the function $\hat{y}(\hat{t})$ depends a priori on both parameters $\hat{w}$ and $\hat{v}_0$. In order to determine this functional dependence, which is not known *a priori*, we rescale the time variable. The choice of a relevant time scale is not obvious, however. Indeed, while the inverse of the shear rate yields a natural scale, this is not an adequate choice since the shear rate is not constant along the trajectory. The trick is to rescale each infinitesimal time step $dt$ around the time $t$ by the local shear rate $\dot{\gamma}(y) = dv^\infty/dy = c(w - y)$ of the unperturbed flow at the position $y(t)$. The new dimensionless time-like parameter is then obtained by integrating the rescaled time steps: $\tilde{t} = \int_0^t \dot{\gamma}(y)dt' = c\int_0^t \left[w - y(t')\right]dt'$. $\tilde{t}$ accounts for the history of the shear rates experienced by the vesicle along its trajectory. The raw data (not shown) for the migration velocity spreads over more than a decade in the parameters space. Interestingly, as shown in Fig. 1(b), all experimental curves $\hat{y}(\tilde{t})$ for a given $\nu$ (or rather, a tiny interval around it) collapse, whatever the values of $\hat{w}$ and $\hat{v}_0$ within the explored range. A log-log plot (not shown) of each master curve $\hat{y}(\tilde{t}) - \hat{y}_0$ is linear, a clear signature of a power law behavior $\hat{y}(\tilde{t}) - \hat{y}_0 = \beta\tilde{t}^\alpha$, where the dimensionless parameters $\alpha$ and $\beta$ are thus independent from $\hat{w}$ and $\hat{v}_0$. The lateral migration velocity $\hat{v}_m \equiv \dot{\hat{y}}$ as a function of the position $\hat{y}$ and $(\hat{w}, \hat{v}_0)$ is then easily extracted:

$$\hat{v}_m = \xi\frac{\hat{\dot{\gamma}}(\hat{y})}{(\hat{y} - \hat{y}_0)^\delta}, \quad \text{that is:} \quad \dot{y} = \xi\frac{R_0^{\delta+1}\dot{\gamma}(y)}{(y - y_0)^\delta}. \quad (1)$$

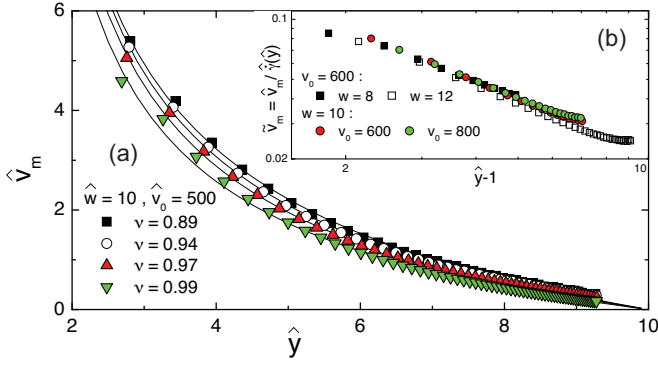This law constitutes the central result of our finding. In the range $0.970 < \nu < 0.975$ we find for

FIG. 2: (color online) Simulations. (a): migration velocity $\hat{v}_m$ versus lateral position for different reduced volumes. Solid lines show the fits to Eq. 1. (b): log-log plot of $\tilde{v}_m$ versus $\hat{y}-1$ for different $\hat{w}$ and $\hat{v}_0$ and $\nu = 0.97$.
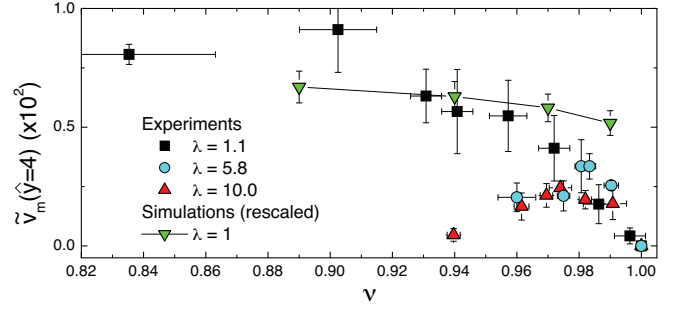


FIG. 3: (color online) Reduced migration velocity $\tilde{v}_m$ of a vesicle at position $\hat{y} = 4$ versus its reduced volume. For readability, the simulations data are uniformly rescaled by a factor $\sim 0.1$.

instance $\xi \equiv \alpha\beta^{1/\alpha} = 1.2 \times 10^{-2} \pm 0.2 \times 10^{-2}$ and $\delta \equiv 1/\alpha - 1 = 1 \pm 0.1$. The error bars for these coefficients are mainly due to the uncertainties on the measure of $\nu$, of order $\pm 0.005$, since, as we shall see, the velocity depends on the reduced volume. Note that the differential equation 1 has no analytical solution but can be easily solved numerically and the result used to fit the raw data $y(t)$ without rescaling procedure (Fig. 1(a)).

In the simulations, we studied 2D neutrally buoyant vesicles (the 2D geometry captures the essential features) having no viscosity contrast ($\lambda = 1$). The fluids flows inside and outside the vesicle are governed by the Stokes equations ($\mathbf{r_m} \in \partial\Omega$ is a membrane point):

$$-\nabla p(\mathbf{r}) + \eta\nabla^2\mathbf{v}(\mathbf{r}) = -\delta(\mathbf{r}-\mathbf{r_m})\mathbf{f}(\mathbf{r}), \ \nabla\cdot\mathbf{v}(\mathbf{r}) = 0, \ (2)$$

where $p$ is the pressure, $\mathbf{v}$ is the velocity and $\mathbf{f}$ the membrane force, given by Eq. 8 of Ref. [27]. Thanks to the linearity of Eqs. 2, we solve them using a boundary integral method [29] adapted to vesicle problems [7, 24, 27, 30]. The membrane velocity is then given by the following integral equation, that we solve numerically:

$$v_i(\mathbf{r_m}) = \frac{1}{4\pi\eta}\oint_{\partial\Omega}\mathbf{G}_{ij}^W(\mathbf{r_m},\mathbf{r}')f_j(\mathbf{r}')ds(\mathbf{r}')+v_i^\infty(\mathbf{r_m}), \ (3)$$

where $\mathbf{G}_{ij}^W$ is the Green's function for a fluid bounded by a steady infinite plane wall located at $y = 0$:

$$\mathbf{G}_{ij}^W(\mathbf{r},\mathbf{r}') = \mathbf{G}_{ij}(\mathbf{r}-\mathbf{r}') - \mathbf{G}_{ij}(\mathbf{r}-\mathbf{r}'_I)$$
$$+ \ 2r_y'^2\mathbf{G}_{ij}^D(\mathbf{r}-\mathbf{r}'_I) - 2r_y'\mathbf{G}_{ij}^{SD}(\mathbf{r}-\mathbf{r}'_I). \ (4)$$

$\mathbf{G}_{ij}(\mathbf{r}) = -\delta_{ij}\ln r + \frac{r_ir_j}{r^2}$ is the Green's function for an unbounded fluid, or Stokeslet, $\mathbf{r}'_I = (r'_x, -r'_y)$ is the image of $\mathbf{r}'$ with respect to the wall. The function

$$\mathbf{G}_{ij}^D(\mathbf{r}) = (\delta_{jx} - \delta_{jy})\left(\frac{\delta_{ij}}{r^2} - 2\frac{r_ir_j}{r^2}\right) \qquad (5)$$

is the Stokeslet doublet, and the source doublet is

$$\mathbf{G}_{ij}^{SD}(\mathbf{r}) = r_y\mathbf{G}_{ij}^D(\mathbf{r}) + (\delta_{jx} - \delta_{jy})\frac{\delta_{jy}r_i - \delta_{iy}r_j}{r^2}. \qquad (6)$$

The evolution of the vesicle's shape and location are obtained by updating every membrane point using a Euler scheme: $\mathbf{r_m}(t + \Delta t) = \mathbf{v}(\mathbf{r_m}, t)dt + \mathbf{r_m}(t)$.

Note that we only consider one wall at $y = 0$. Provided $\hat{w} \geq 8$, the vesicle reaches and stays on the $\hat{y} = \hat{w}$ line at long times, even without the symmetric wall at $\hat{y} = 2\hat{w}$. This seems to indicate that for $\hat{w} \geq 8$, migration forces due to the curvature dominate over wall effects near the center-line.

The variations of $\hat{v}_m$ with $\hat{y}$ are shown in Fig. 2(a) for four different reduced volumes and given width and flow velocity. They are well described by Eq. 1. The adequation to this law is confirmed by considering varying $8 < \hat{w} < 12$ and $600 < \hat{v}_0 < 800$. Following Eq. 1, it is convenient to rescale the migration velocity in such a way that it should not depend either on $\hat{w}$, nor on $\hat{v}_0$: $\tilde{v}_m \equiv \hat{v}_m/\hat{\dot{\gamma}}(\hat{y}) = \xi/(\hat{y} - \hat{y}_0)^\delta$. The variations of $\tilde{v}_m$ with $\hat{y} - 1$ are shown in Fig. 2(b) for $\nu = 0.97$. The collapse on a single line (in log-log scale) is in accordance with Eq. 1. We find $\delta \simeq 0.8 \pm 0.1$ and $\xi \simeq 0.1$. The agreement between experiments and simulations regarding the exponent $\delta$ is quite satisfactory. However, numerical studies overestimate the amplitude $\xi$. This is attributed to the 2D character (actually a translationally invariant form in the $z$ direction), causing an enhancement of the lift force. While 2D simulations have captured some interesting facts, a 3D simulation is necessary before drawing general conclusive answers, and we plan to investigate this problem in the future.

We now discuss the dependencies on $\nu$ and $\lambda$; for all the values of $\nu$ and $\lambda$ explored here, the experimental and numerical curves are still very well fitted by the law given by the resolution of Eq. 1 (see Fig. 1(a)). Values for $\tilde{v}_m$ at $\hat{y} = 4$ are reported on Fig. 3. For $\lambda \simeq 1$, in the ranges $0.83 \leq \nu \leq 1$ and $0.89 \leq \nu \leq 0.99$ offered respectively by the experiments and the simulations, we find an increasing migration velocity with decreasing $\nu$ (as seen on Fig. 2(a)).

Results for higher $\lambda$ are available from the experiments. The new feature is the non monotonous behavior of $\tilde{v}_m$ as a function of $\nu$. When $\nu$ is decreased from 1, the

migration velocity first increases (as for $\lambda = 1.1$), then reaches a maximum and decreases back to a very low value (Fig. 3).

This non-monotonous behavior of the velocity can be understood on a general physical basis. A spherical vesicle ($\nu = 1$), does not migrate owing to the fore-aft symmetry. On the other hand, when $\nu$ decreases, the vesicle finally switches from a tank-treading to a tumbling motion [12]. In the latter regime, no global migration should occur either because the averaging over the different orientations of the vesicle during one rotation period leads to an almost symmetrical configuration. From these considerations we infer a maximal velocity at a given value of $\nu$. Note that when $\lambda \simeq 1$, no tumbling motion occurs whatever $\nu$, so that a monotonous evolution of the velocity with $\nu$ is observed. The evolution with $\nu$ and $\lambda$ is in qualitative agreement with the predictions made by Olla for the migration velocity of a (shape preserving ellipsoidal) vesicle in the case of a simple shear flow bounded by a wall, although the scaling is different [22].

In conclusion, our experiments and simulations yield a similarity law for the lateral migration velocity of a vesicle in a bounded Poiseuille flow as a function of its distance to the walls and to the center-line, its effective radius, the channel's width and the flow velocity. We showed that the effects of the walls and of the curvature of the velocity field are coupled in a non linear manner: curvature not only induces migration [27] but also affects the shape and orientation, which affects the lift force. The law $v_m \sim \dot{\gamma}(y)/y$ markedly differs from what the naive extrapolation of the results for a vesicle near a wall and in a linear shear flow would give: $v_m \sim \dot{\gamma}(y)/y^2$.

Deflating a spherical vesicle increases its deformability, thus its asymmetry under shear, and leads to higher migration velocities. However, beyond a given viscosity ratio, the tank-treading to tumbling transition is approached when the deflation increases, and the migration velocity undergoes a decline which can be understood on the ground of general symmetry considerations.

[1] E. S. Asmolov, The inertial lift on a small particle in a weak-shear parabolic flow, Phys. Fluids **14**, 15 (2002).

[2] S. Eloot, F. De Bisschop, and P. Verdonck, Experimental evaluation of the migration of spherical particles in three-dimensional Poiseuille flow, Phys. Fluids, **16**, 2282 (2004).

[3] Y. W. Kim and J. Y. Yoo, The lateral migration of neutrally-buoyant spheres transported through square microchannels, J. Micromech. Microeng.. **18**, 65015 (2008).

[4] Y. C. Fung, *Biomechanics; mechanical properties of living tissues* (Springer, Berlin, 1993).

[5] N. Pamme, Continuous flow separations in microfluidic devices, Lab on a chip **7**, 1644 (2007).

[6] J. R. Keller and R. Skalak, Motion of a tank-treading ellipsoidal particle in a shear flow, J. Fluid Mech. **120**, 27 (1982).

[7] J. Beaucourt, F. Rioual, T. Séon, T. Biben, and C. Misbah, Steady to unsteady dynamics of a vesicle in a flow, Phys. Rev. E **69**, 011906 (2004).

[8] C. Misbah, Vacillating Breathing and Tumbling of Vesicles under Shear Flow, Phys. Rev. Lett. **96**, 028104 (2006).

[9] P. M. Vlahovska and R. Serral Gracia, Dynamics of a viscous vesicle in linear flows, Phys. Rev. E **75**, 016313 (2007).

[10] H. Noguchi and G. Gompper, Swinging and tumbling of fluid vesicles in shear flow, Phys. Rev. Lett. **98**, 128103 (2007).

[11] K. H. de Haas, C. Blom, D. van den Ende, M. H. G. Duits, and J. Mellema, Deformation of giant lipid bilayer vesicles in shear flow, Phys. Rev. E **56**, 7132 (1997).

[12] M.-A. Mader, V. Vitkova, M. Abkarian, A. Viallat, and T. Podgorski, Dynamics of viscous vesicles in shear flow, Eur. Phys. J. E **19**, 389 (2006).

[13] V. Kantsler and V. Steinberg, Transition to Tumbling and Two Regimes of Tumbling Motion of a Vesicle in Shear Flow, Phys. Rev. Lett., **96**, 036001 (2006).

[14] R. Bruinsma, Rheology and shape transitions of vesicles under capillary flow, Physica A **234**, 249 (1996).

[15] V. Vitkova, M.-A. Mader, and T. Podgorski, Deformation of vesicles flowing through capillaries, Europhys. Lett. **68**, 398 (2004).

[16] H. Noguchi and G. Gompper, Vesicle dynamics in shear and capillary flows, J. Phys. Cond. Matter **17**, S3439 (2005).

[17] F. Risso, F. Collé-Paillot, and M. Zagzoule, Experimental investigation of a bioartificial capsule flowing in a narrow tube, J. Fluid. Mech. **547**, 149 (2006).

[18] T. W. Secomb, B. Styp-Rekowska, and A. R. Pries, Two-dimensional simulation of red blood cell deformation and lateral migration in microvessels, Ann. Biomed. Eng. **35**, 755 (2007).

[19] P. Bagchi, Mesoscale Simulation of Blood Flow in Small Vessels, Biophys. J. **92**, 1858 (2007).

[20] S. Mortazavi and G. Tryggvason, A numerical study of the motion of drops in Poiseuille flow. Part 1. Lateral migration of one drop, J. Fluid Mech. **411**, 325 (2000).

[21] A. J. Griggs, A. Z. Zinchenko, and R. H. Davis, Low-Reynolds-number motion of a deformable drop between two parallel plane walls, Int. J. Mult. Flow **33**, 182 (2007).

[22] P. Olla, The lift on a tank-treading ellipsoidal cell in a shear flow, J. Phys. II France **7**, 1533 (1997).

[23] I. Cantat and C. Misbah, Lift Force and Dynamical Unbinding of Adhering Vesicles under Shear Flow, Phys.

Rev. Lett. **83**, 880 (1999).

[24] S. Sukumaran and U. Seifert, Influence of shear flow on vesicles near a wall: a numerical study, Phys. Rev. E **64**, 011916 (2001).

[25] M. Abkarian, C. Lartigue, and A. Viallat, Tank Treading and Unbinding of Deformable Vesicles in Shear Flow: Determination of the Lift Force, Phys. Rev. Lett. **88**, 068103 (2002).

[26] N. Callens, C. Minetti, G. Coupier, M.-A. Mader, F. Dubois, C. Misbah, and T. Podgorski, Hydrodynamic lift of vesicles under shear flow in microgravity, Europhys. Lett. **83**, 24002 (2008).

[27] B. Kaoui, G. Ristow, I. Cantat, C. Misbah, and W. Zim-mermann, Lateral migration of a two-dimensional vesicle in unbounded Poiseuille flow, Phys. Rev. E **77**, 021903 (2008).

[28] F. M. White, *Viscous Fluid Flow* (McGraw-Hill, New-York, 1991).

[29] C. Pozrikidis, *Boundary Integral and Singularity Methods for Linearized Viscous Flow* (Cambridge University Press, Cambridge, 1992).

[30] I. Cantat, K. Kassner, and C. Misbah, Vesicles in hapto-taxis with hydrodynamical dissipation, Eur. Phys. J. E **10**, 175 (2003).